

Movements of the ϵ -subunit during catalysis and activation in single membrane-bound H^+ -ATP synthase

Boris Zimmermann¹, Manuel Diez¹,
Nawid Zarrabi², Peter Gräber¹ and
Michael Börsch^{2,*}

¹Institut für Physikalische Chemie, Albert-Ludwigs-Universität Freiburg, Freiburg, Germany and ²3. Physikalisches Institut, Universität Stuttgart, Stuttgart, Germany

F₀F₁-ATP synthases catalyze proton transport-coupled ATP synthesis in bacteria, chloroplasts, and mitochondria. In these complexes, the ϵ -subunit is involved in the catalytic reaction and the activation of the enzyme. Fluorescence-labeled F₀F₁ from *Escherichia coli* was incorporated into liposomes. Single-molecule fluorescence resonance energy transfer (FRET) revealed that the ϵ -subunit rotates stepwise showing three distinct distances to the *b*-subunits in the peripheral stalk. Rotation occurred in opposite directions during ATP synthesis and hydrolysis. Analysis of the dwell times of each FRET state revealed different reactivities of the three catalytic sites that depended on the relative orientation of ϵ during rotation. Proton transport through the enzyme in the absence of nucleotides led to conformational changes of ϵ . When the enzyme was inactive (i.e. in the absence of substrates or without membrane energization), three distances were found again, which differed from those of the active enzyme. The three states of the inactive enzyme were unequally populated. We conclude that the active–inactive transition was associated with a conformational change of ϵ within the central stalk.

The EMBO Journal (2005) 24, 2053–2063. doi:10.1038/sj.emboj.7600682; Published online 26 May 2005

Subject Categories: structural biology; membranes & transport

Keywords: ϵ -subunit; F₀F₁-ATP synthase; fluorescence resonance energy transfer; rotation; single-molecule enzymology

Introduction

ATP is synthesized by F-type ATP synthases in the plasma membrane of bacteria, the inner membrane of mitochondria, and the thylakoid membrane of chloroplasts. These multi-subunit enzymes consist of two major complexes with distinct functionalities: the hydrophobic membrane-integrated F₀ part (subunits *ab*₂*c*₁₀ in *Escherichia coli*) is involved in proton transport across the membrane, and the hydrophilic F₁

part (subunits $\alpha_3\beta_3\gamma\delta\epsilon$) contains the three catalytic nucleotide and phosphate binding sites (Yoshida *et al.*, 2001; Capaldi and Aggeler, 2002; Weber and Senior, 2003; Kinoshita *et al.*, 2004). F₀ and F₁ parts are connected by a central and a peripheral stalk, as revealed by electron micrographs (Böttcher *et al.*, 1998; Wilkens and Capaldi, 1998; Karrasch and Walker, 1999). The central stalk is built by the γ - and ϵ -subunit of F₁, and parts of both subunits are interfacing the ring of *c*-subunits of F₀. ATP synthesis takes place at the catalytic sites on the β -subunits. The Gibbs free energy derived from the electrochemical potential of the proton gradient across the membrane is transduced via conformational changes to the catalytic nucleotide binding sites (Junge, 1999; Capaldi and Aggeler, 2002; Weber and Senior, 2003), where it is used to alter the binding affinities of substrates and products as proposed by the ‘binding change mechanism’ (Boyer, 1998). During ATP synthesis, translocation of protons through F₀ drives rotation of the ‘rotor’-subunits $\gamma\epsilon c_{10}$ (blue in Figure 1A) relative to the ‘stator’-subunits $\alpha_3\beta_3\delta ab_2$ (orange in Figure 1A) (Zhou *et al.*, 1997; Kaim *et al.*, 2002; Boldt *et al.*, 2004; Diez *et al.*, 2004b). The actual conformational state of each of the three catalytic sites depends on the orientation of the ‘rotor’ subunits relative to the $\alpha\beta$ -pairs. Rotation of the γ -subunit has been observed with molecule ensembles (Duncan *et al.*, 1995; Sabbert *et al.*, 1996) and with single immobilized F₁ subcomplexes (Noji *et al.*, 1997; Yasuda *et al.*, 2001). Rotation of the γ -subunit relative to the *b*-subunit (stator) has been observed with a single membrane-bound F₀F₁-ATP synthase in liposomes using fluorescence resonance energy transfer (FRET) (Börsch *et al.*, 2002). Recently, a three-stepped rotation of the γ -subunit was reported during coupled catalysis with opposite directions during ATP synthesis and ATP hydrolysis (Diez *et al.*, 2004b).

Not much data have been reported about movements of the ϵ -subunit. Crosslinking of the γ - and ϵ -subunits does not impair ATP hydrolysis in molecule ensembles (Tang and Capaldi, 1996; Aggeler *et al.*, 1997; Bulygin *et al.*, 1998), indicating that ϵ is part of the rotor. Rotation of the ϵ -subunit in single immobilized F₁ parts during ATP hydrolysis was demonstrated (Häsler *et al.*, 1998; Kato-Yamada *et al.*, 1998). However, these experiments did not reveal a 120° stepped rotation as for the γ -subunit and give no conclusive evidence for a joint rotation of the $\gamma\epsilon$ -complex. The ϵ -subunit is also involved in the activation of the enzyme, and the active–inactive transition is a complex process that depends on several parameters including the number and type of the enzyme-bound nucleotides, energization of the membrane, and the dissociation of ϵ (Smith and Sternweis, 1977; Fischer *et al.*, 2000). Finally, the ϵ -subunit might play an important role in switching between the ATP synthesis and ATP hydrolysis mode (Tsunoda *et al.*, 2001). In this work, we used a single-molecule FRET approach to investigate the movements of the ϵ -subunit in the membrane-bound H^+ -ATP synthases from *E. coli* during proton transport-driven ATP synthesis and

*Corresponding author. 3. Physikalisches Institut, Universität Stuttgart, Pfaffenwaldring 57, 70569 Stuttgart, Germany.
Tel.: +49 711 685 4632; Fax: +49 711 685 5281;
E-mail: m.boersch@physik.uni-stuttgart.de

Received: 18 January 2005; accepted: 26 April 2005; published online: 26 May 2005

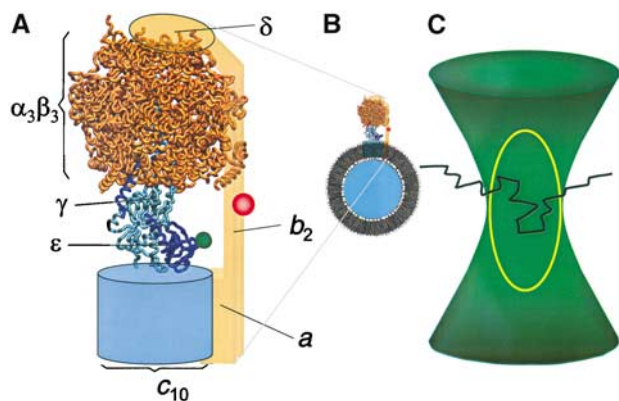


Figure 1 Model of the H^+ -ATP synthase from *E. coli* as derived from electron microscopic data (Böttcher *et al*, 2000; Rubinstein *et al*, 2003), the homology model of F_1 (Engelbrecht and Junge, 1997), and the structure of the $\gamma\epsilon$ -complex (Rodgers and Wilce, 2000). (A) The H^+ -ATP synthase is labeled with the FRET donor TMR (green) at the ϵ -subunit and the FRET acceptor Cy5bis (red) at the b -subunits. 'Rotor' subunits are depicted in blue and 'stator' subunits are orange. (B) F_0F_1 incorporated into a liposome membrane. The diameter of the F_1 part is 10 nm and that of the liposome is 120 nm. Liposomes used for FRET analysis contained one F_0F_1 . (C) Photon bursts from the FRET-labeled F_0F_1 are observed when the liposome traverses the confocal detection volume (yellow line) within the excitation focus (green) of the laser. A schematic diffusion pathway of the liposome through the confocal volume is indicated (black line).

hydrolysis, and we discriminated movements during catalysis from those during activation.

Results

Labeling of F_0F_1 and fluorescence measurements with single enzymes

To investigate the movements of the ϵ -subunit, we prepared H^+ -ATP synthase from *E. coli* (referred to as F_0F_1 in the following) in freely diffusing lipid vesicles. We monitored rotation of the ϵ -subunit relative to the b -subunits during ATP synthesis and ATP hydrolysis using single-molecule FRET. The 'rotor'-subunit ϵ of F_1 was labeled with tetramethylrhodamine (TMR) as the FRET donor to yield F_1 - ϵ H56C-TMR. A bisfunctional cyanine dye, Cy5bis (Diez *et al*, 2004b), was used as the FRET acceptor, which crosslinked the dimeric 'stator'-subunits b_2 of F_0F_1 to yield F_0 - b Q64C-Cy5bis- F_1 . The SDS gel (Figure 2) shows F_0F_1 before labeling (lane 1a), and F_0F_1 after labeling with Cy5bis (lane 2a), indicating the crosslinking of subunit b (marked b_2). The fluorogram (lane 2b) reveals selective labeling of b_2 . Lane 3a shows F_1 after labeling with TMR; the fluorogram (lane 3b) indicates selective labeling of ϵ . To obtain specifically double-labeled F_0F_1 , the following procedure was used (for details, see Materials and methods): F_0 - b Q64C-Cy5bis- F_1 was incorporated into liposomes, and the F_1 part was removed. The liposomes with the membrane-bound Cy5bis-labeled F_0 part were reassembled with F_1 - ϵ H56C-TMR. Proteoliposomes with double-labeled F_0F_1 were obtained (see Figure 1B) after removal of excess F_1 - ϵ H56C-TMR. In control experiments, we used unlabeled enzymes for incorporation into liposomes, removal of F_1 , and reassembling with new unlabeled F_1 . At each step of the preparation of both sample and control, the rates of ATP hydrolysis (ν_H) and ATP synthesis (ν_S) were

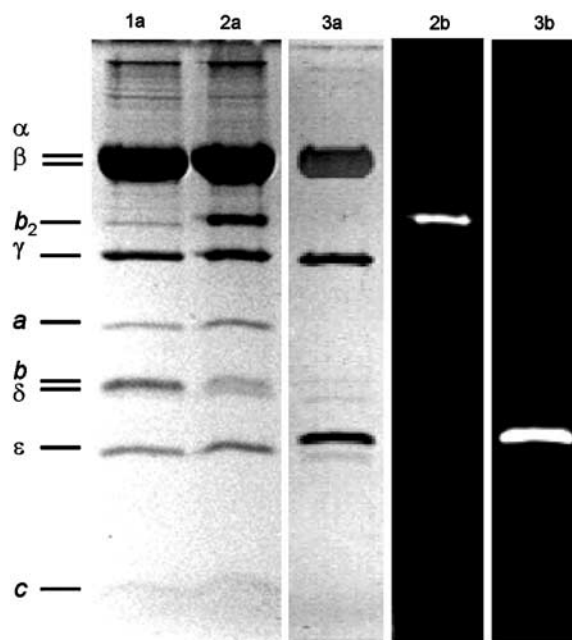


Figure 2 SDS-PAGE (13%) of F_1 and F_0F_1 . Lanes marked with (a) show the protein stained with Coomassie blue and those marked with (b) show the corresponding fluorograms. Lane 1: F_0 - b Q64C- F_1 ; lane 2: F_0 - b Q64C-Cy5bis- F_1 showing crosslinking of subunits b by Cy5bis; lane 3: F_1 - ϵ H56C-TMR.

measured. The results are summarized in Table I and show that the rates of ATP hydrolysis and ATP synthesis are not changed when the enzyme is labeled either with TMR at the ϵ -subunit or with Cy5bis at the b -subunit. The ATP synthesis activity of F_0 - b Q64C-Cy5bis- F_1 is decreased by approximately 50% after removal and rebinding of F_1 ; however, there is no difference in activity between labeled and unlabeled F_1 . Double-labeled enzymes show catalytic rates of $\nu_H = 57 \pm 19 \text{ s}^{-1}$ corresponding to a mean turnover time of $t_H = 18 \pm 4 \text{ ms}$, and $\nu_S = 21 \pm 4 \text{ s}^{-1}$ corresponding to a mean turnover time of $t_S = 48 \pm 8 \text{ ms}$. Addition of *N,N'*-dicyclohexylcarbodiimide (DCCD), which binds covalently to the c -subunits, inhibits both ATP synthesis and ATP hydrolysis.

Single-molecule FRET measurements of the membrane-integrated H^+ -ATP synthases with selectively attached fluorophores were carried out in a confocal setup with two-channel detection (Börsch *et al*, 2002). TMR was excited at 532 nm, and the emission of both fluorophores was simultaneously recorded. Fluorescence of TMR was detected in the spectral range between 545 and 610 nm (F_D), and of Cy5bis above 660 nm (F_A). Well-separated photon bursts with count rates up to 100 photons/ms were observed when a single liposome containing one double-labeled F_0F_1 diffused through the confocal detection volume as shown schematically in Figure 1C. Time-dependent fluctuations of the fluorescence intensities in both channels reflect the stochastic pathway of the liposome through the confocal volume. This volume can be approximated by a three-dimensional Gaussian excitation intensity distribution (green in Figure 1C) and a confocal detection volume of the fluorescence emission (yellow in Figure 1C). The FRET efficiency $E_{\text{FRET}} = F_A / (F_A + F_D)$ calculated from the ratio of corrected fluorescence intensities in the donor channel (F_D) and the acceptor channel (F_A) is independent of the localization within the

Table 1 Rates of ATP hydrolysis (v_H) and ATP synthesis (v_S) of liposome-bound F_0F_1 at 23°C, measured at different states during the preparation procedure

Enzymes	v_H (s^{-1})		v_S (s^{-1})	
		+ DCCD		+ DCCD
F_0F_1 'wild type'	91 ± 2	ND	87 ± 11	ND
F_0 -bQ64C- F_1	71 ± 4	ND	60 ± 1	ND
F_0 -bQ64C-Cy5bis- F_1	75 ± 9	ND	48 ± 1	ND
F_0 -bQ64C (after removal of F_1)	0	ND	0	ND
F_0 -bQ64C-Cy5bis (after removal of F_1)	0	ND	0	ND
F_0 -bQ64C- F_1 , after removal of F_1 and reassembling with F_1 - ϵ H56C	55 ± 8	4 ± 2	22 ± 3	4 ± 3
F_0 -bQ64C- F_1 , after removal of F_1 and reassembling with F_1 - ϵ H56C-TMR	55 ± 9	5 ± 1	21 ± 3	4 ± 2
F_0 -bQ64C-Cy5bis after removal of F_1 and reassembling with F_1 - ϵ H56C	52 ± 8	5 ± 1	23 ± 3	5 ± 2
F_0 -bQ64C-Cy5bis after removal of F_1 and reassembling with F_1 - ϵ H56C-TMR	57 ± 19	5 ± 2	21 ± 4	4 ± 0

ND: not determined.

confocal volume. Therefore, a constant ratio of the fluorescence intensities throughout a photon burst indicated a constant E_{FRET} that corresponds to a fixed distance between the two fluorophores. The distance can be calculated according to the Förster theory of FRET (Förster, 1948; Van der Meer *et al*, 1994).

Fluorescence trajectories and dynamics of ϵ -subunit movement during catalysis

In the presence of 1 mM AMPPNP (an ATP analog that is bound at the catalytic sites but is not hydrolyzed), the photon bursts simultaneously exhibited large changes in fluorescence intensities of FRET donor and acceptor due to the diffusion through the confocal volume as shown in Figure 3A (F_D , green trajectories; F_A , red trajectories). The FRET efficiency E_{FRET} calculated from these trajectories (blue trace) remained unchanged within the bursts, indicating a constant distance of the ϵ -subunit with respect to the b -subunits during the observation time. We observed three different FRET states, one with low FRET efficiency (L), one with medium FRET efficiency (M), and one with high FRET efficiency (H). In addition, Figure 3A shows a photon burst resulting from an enzyme carrying only the donor fluorophore (D). In all trajectories, the mean background counts were subtracted in each channel, and, therefore, the acceptor channel count rate of a donor-only-labeled enzyme is zero as well as the FRET efficiency.

During ATP hydrolysis in the presence of 1 mM ATP, large fluctuations in fluorescence intensities of donor and acceptor were observed within single photon bursts (Figure 3B). Three different FRET levels were found with similar FRET efficiencies as in the presence of AMPPNP, which were called also L, M, and H. However, we detected often more than one FRET level per photon burst. The time traces of the FRET efficiency (blue traces) show distinct FRET levels (between 5 and 150 ms) but in contrast to the AMPPNP case, there were rapid changes to the next FRET level. The stepping occurred faster than the time resolution of these measurements (1 ms). We analyzed photon bursts that showed at least one FRET transition (two FRET levels). In 454 photon bursts, we found FRET level transitions with the sequence $\rightarrow H \rightarrow M \rightarrow L \rightarrow H \dots$ for more than 81% of the bursts, and 19% showed apparently the wrong sequence (details of the statistics are provided as Supplementary data). From these data, it can be concluded that the distances between the ϵ -subunit and the b -subunits

change sequentially in one direction, and this implies a three-stepped rotary movement of ϵ relative to b .

To investigate ATP synthesis, a pH difference plus an additional electric potential difference was generated across the liposome membrane in the presence of 100 μ M Mg-ADP and 5 mM phosphate (see Materials and methods). We measured the rate of ATP synthesis with luciferin/luciferase under these conditions in ensemble experiments, and found ATP synthesis activity up to 3 min. Therefore, the single-molecule data were collected for 3 min after energization. During ATP synthesis, again three different FRET states were observed at similar levels as during ATP hydrolysis, and with rapid changes between them (Figure 3C). The sequence $\rightarrow L \rightarrow M \rightarrow H \rightarrow L \dots$ of FRET states was found for 84% of 386 analyzed bursts with at least one FRET transition. These data indicate unidirectional sequential changes in the distances between the two fluorophores, that is, rotation of the ϵ -subunit relative to the b -subunits in three steps during ATP synthesis, and in the opposite direction as observed during ATP hydrolysis.

To investigate the movements of the ϵ -subunit during proton transport without ATP synthesis or ATP hydrolysis, the proteoliposomes were energized by Δ pH and $\Delta\phi$ in the absence of nucleotides. Figure 3D shows two examples of photon bursts under these conditions. Three similar FRET efficiencies were discriminated as during ATP hydrolysis and ATP synthesis, which changed rapidly. However, the sequence in synthesis direction was found for 66% of 140 analyzed bursts with at least two FRET levels, and 34% rotated in hydrolysis direction, with a mean dwell time of $t_E = 38 \pm 8$ ms.

Donor-acceptor distances and populations of the three FRET states

For a statistical evaluation of all photon bursts, the mean E_{FRET} value of each FRET level during ATP hydrolysis, ATP synthesis, proton transport, and AMPPNP binding was calculated and is shown as black lines in Figure 3. The resulting FRET level histograms are depicted in Figure 4. All histograms exhibited three peaks, and each peak was fitted with a Gaussian distribution (for details, see Supplementary data). From the maxima of each peak, the most probable donor-acceptor distance (r_{DA}) was calculated using $E_{\text{FRET}} = (R_0)^6 / [(R_0)^6 + (r_{\text{DA}})^6]$ and a Förster radius $R_0 = 6.4$ nm for the pair TMR at ϵ and Cy5 at b_2 (see Materials and methods). The maxima of the three FRET levels were found at approximately the same FRET efficiencies during ATP hydrolysis, ATP

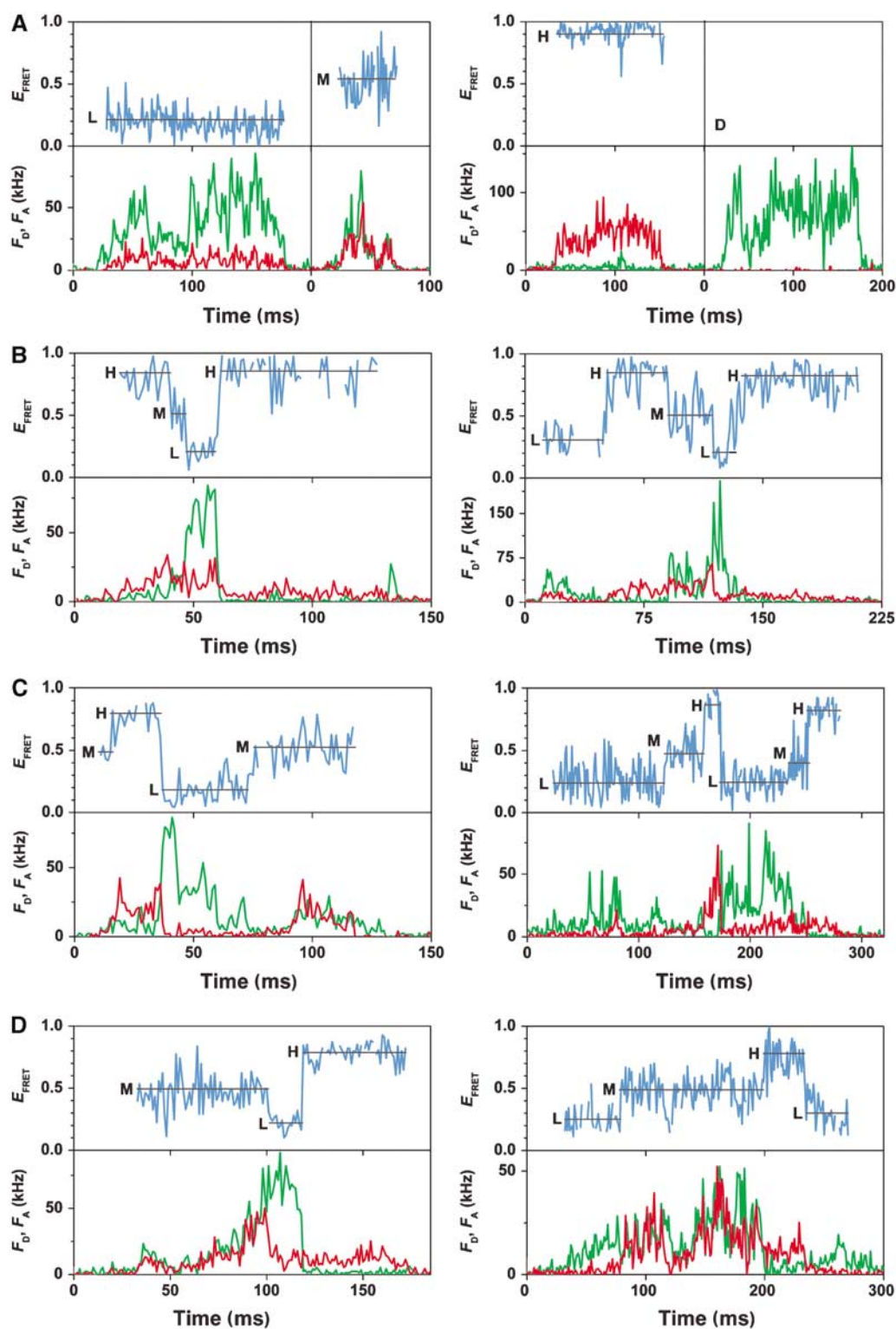


Figure 3 Photon bursts of FRET-labeled F_0F_1 in liposomes. Corrected fluorescence intensity traces of the donor, F_D , and acceptor, F_A , are green and red, respectively. The FRET efficiencies (E_{FRET}) calculated from these traces are shown as blue traces. For each FRET level, the arithmetic mean value is calculated (black line). The three FRET states are labeled L, M, and H. (A) Traces in the presence of AMPPNP showing constant FRET efficiencies and a donor-only-labeled F_0F_1 in a liposome (D). (B) Traces during ATP hydrolysis showing stepwise changes of FRET levels in the sequence $\rightarrow L \rightarrow H \rightarrow M \rightarrow L$. (C) Traces during ATP synthesis showing stepwise changes of FRET levels in the sequence $\rightarrow L \rightarrow M \rightarrow H \rightarrow L$. (D) Traces during proton transport showing both sequences.

synthesis, and proton transport (Figure 4B–D). These efficiencies corresponded to distances between donor and acceptor of 7.8 nm (L), 6.3 nm (M), and 4.6 nm (H).

In the presence of AMPPNP, no catalysis takes place, and, correspondingly, no changes of FRET levels during the photon bursts were observed. Still the maxima of the

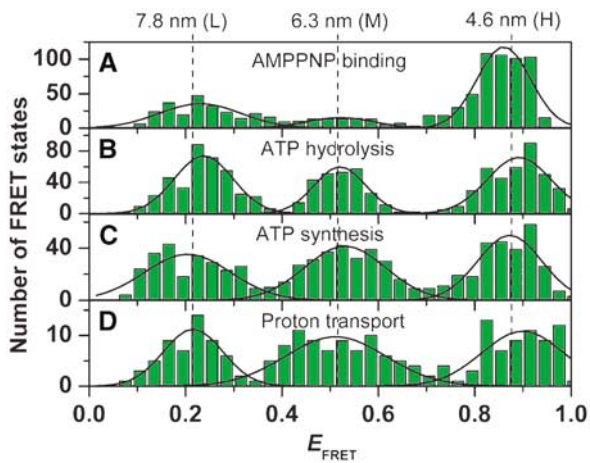


Figure 4 Histograms of the FRET efficiencies for the active F_0F_1 . The mean FRET efficiency was calculated for each observed FRET level (see black lines in Figure 3) and the number of observations was plotted as a function of E_{FRET} . (A) In the presence of AMPPNP (data from 888 photon bursts). (B) ATP hydrolysis (454 photon bursts). (C) ATP synthesis (368 photon bursts). (D) proton transport (140 photon bursts). The peaks were fitted by Gaussian distributions. For all conditions, the maxima of the distributions are observed at the same FRET efficiency (black lines). The calculated distances are shown at the top.

Gaussian distributions give similar distances as during catalysis (Figure 4A). Obviously, the three different FRET distances during catalysis are frozen by AMPPNP binding.

The turnover time of catalysis at the different $\alpha\beta$ -pairs

The dwell time of a FRET state is the duration of a constant ϵ conformation in F_0F_1 during catalysis, and, therefore, it represents the docking time of the $\gamma\epsilon$ -complex to one specific $\alpha\beta$ -pair. In the presence of high nucleotide concentrations (ATP, or ADP plus P_i), this time interval represents, presumably, the time of synthesis or hydrolysis of one ATP at one catalytic site. Switching of the $\gamma\epsilon$ -complex to the next $\alpha\beta$ -pair occurs faster than 1 ms. In Figure 5A the histogram of all dwell times during ATP hydrolysis is shown, and in Figure 5B that of all dwell times during ATP synthesis. Since the dwell times of the first and the last FRET level in a photon burst cannot be determined (because the enzyme in a liposome enters or leaves the confocal volume), only photon bursts with at least two FRET level transitions were used for this analysis. Fitting the distributions during ATP synthesis and hydrolysis monoexponentially yielded mean dwell times $t_S = 17.7 \pm 0.9$ ms and $t_H = 14.3 \pm 0.7$ ms, which are in good agreement with the ensemble turnover times.

According to the binding change mechanism (Boyer, 1993), all three $\alpha\beta$ -pairs carry out consecutively the same reaction steps in a strictly cooperative manner. Thus, it is expected that during steady-state catalysis, each $\alpha\beta$ -pair equally accounts for the catalytic rate. Our data allow for the analysis of the dwell times for each of the three $\alpha\beta$ -pairs separately, that is, the three FRET levels (see insets in Figure 5). During ATP hydrolysis, the M-level has an average dwell time of 12.7 ± 1.0 ms, the L-level 17.6 ± 1.4 ms, and the H-level 15.8 ± 1.7 ms. During ATP synthesis, the M-level has an average dwell time of 15.4 ± 1.0 ms, the L-level 24.0 ± 4.4 ms, and the H-level 19.5 ± 2.2 ms. In both

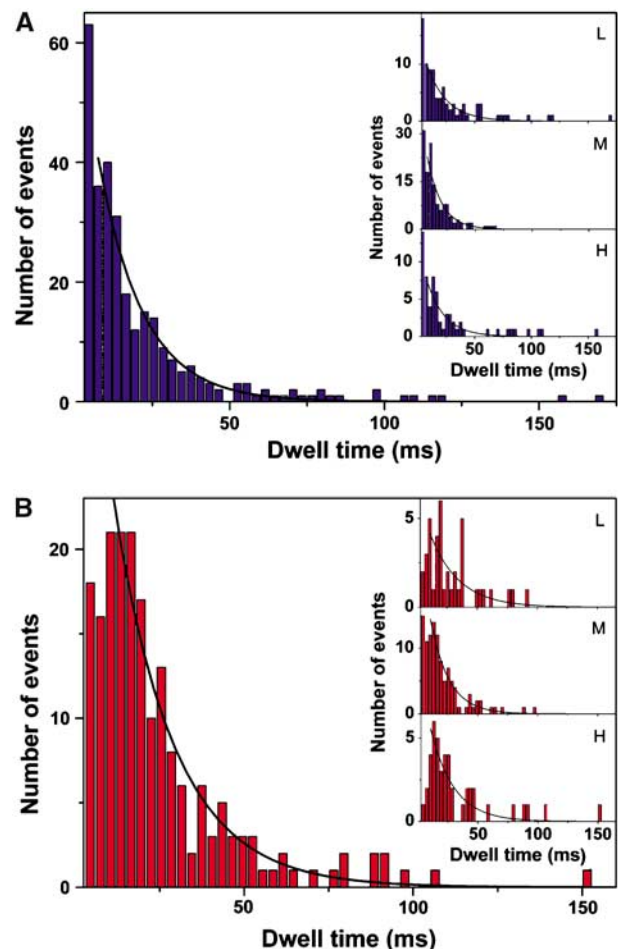


Figure 5 Histograms of dwell times of all FRET levels (A) during ATP hydrolysis (292 dwells) and (B) during ATP synthesis (193 dwells). Monoexponential fits (black lines) yield average dwell times of $t_H = 14.3 \pm 0.7$ ms (mean \pm standard deviation of the mean) during ATP hydrolysis and $t_S = 17.7 \pm 0.9$ ms during ATP synthesis. Monoexponential fits of the dwell times of each FRET level separately (see insets) give $t = 17.6 \pm 1.4$ ms (L, 89 dwells), $t = 12.7 \pm 1.0$ ms (M, 139 dwells), and $t = 15.8 \pm 1.7$ ms (H, 64 dwells) for ATP hydrolysis, and $t = 24.0 \pm 4.4$ ms (L, 41 dwells), $t = 15.4 \pm 1.0$ ms (M, 108 dwells), and $t = 19.5 \pm 2.2$ ms (H, 44 dwells) for ATP synthesis.

directions of catalysis, the M-level exhibits the shortest dwell time.

The docking time of the $\gamma\epsilon$ -complex to one $\alpha\beta$ -pair (that with the medium distance of the label at the ϵ -subunit to the label at the b -subunit) is shorter than the other two. Intrinsically, all $\alpha\beta$ -pairs are identical and they carry out the same catalytic reaction. However, the peripheral stalk with subunits δ and b_2 is attached to one pair (McLachlin *et al*, 2000). Possibly, the conformation of this $\alpha\beta$ -pair differs slightly from the two other pairs, and, accordingly, might effect the required conformational changes for catalysis. This could lead to subtle changes in the Gibbs free energy and the activation barriers for the docking/undocking steps.

Conformational changes of ϵ and the active-inactive transition

Finally, we investigated the enzyme under conditions where it does not carry out catalysis. Different noncatalytic conditions were analyzed and, as in the case of AMPPNP addition (see Figure 3A), photon bursts with a single constant FRET

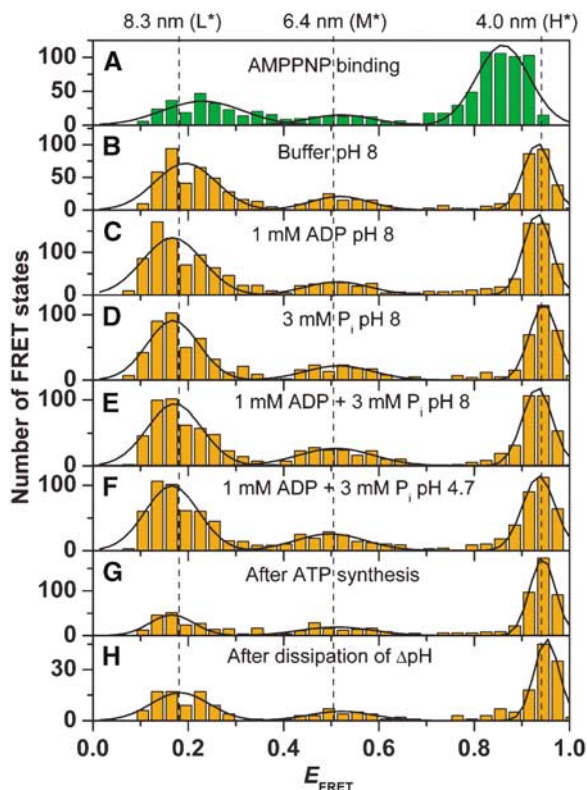


Figure 6 Histograms of the FRET efficiencies for the inactive F_0F_1 . The mean FRET efficiency was calculated for each observed FRET state and the number of observations was plotted as a function of E_{FRET} . For all conditions, the FRET state remained constant during the burst (see Figure 3A). (A) In the presence of AMPPNP (same data as in Figure 4). (B) Buffer, pH 8 (761 photon bursts). (C) Buffer, pH 8, in the presence of ADP (1428 photon bursts). (D) Buffer, pH 8, in the presence of phosphate (869 photon bursts). (E) Buffer, pH 8, in the presence of ADP and phosphate (960 photon bursts). (F) Buffer, pH 4.7, in the presence of ADP and phosphate (985 photon bursts). (G) 5 min after ATP synthesis (755 photon bursts). (H) 5 min after energization with ΔpH and $\Delta\phi$ (230 photon bursts). The peaks were fitted by Gaussian distributions. For all conditions, the same maxima of the distributions are observed (black lines) except for AMPPNP. The calculated distances are shown at the top.

state were observed. We calculated the mean E_{FRET} value for each FRET level, and collected them in histograms for the different experimental conditions (Figure 6). Again, three FRET states were found for F_0F_1 in buffer at pH 8 without substrates, in the presence of ADP or P_i , and in the presence of both ADP and P_i . Since energization of the membrane is achieved by an acid–base transition starting at pH 4.7 (see Materials and methods), we investigated also the enzyme at pH 4.7 (Figure 6F). In addition, FRET level distributions were analyzed after ATP synthesis (Figure 6G) and after dissipation of ΔpH in the absence of substrates (Figure 6H), that is, 5 min after the acid–base transition. The maxima for all ‘inactive’ conditions (with the exception of those in the presence of AMPPNP) were found at different FRET efficiencies compared to those of the catalytically active enzyme. Therefore, we called the three FRET states of the inactive enzymes L^* , M^* , and H^* (for details, see Supplementary data). From the FRET efficiencies of the maxima, donor–acceptor distances of 8.3 nm (L^*), 6.4 nm (M^*), and 4.0 nm (H^*) were calculated. The population of the three inactive FRET states was not equal and differed markedly from that

of active enzymes: without nucleotides as well as in the presence of ADP or P_i (Figure 6B–F), approximately 50% of the enzymes were found in the L^* -state, 15% in the M^* -state, and 35% in the H^* -state. After ATP synthesis (Figure 6E), after proton transport (Figure 6F), and in the presence of AMPPNP (Figure 6A), 30% are in the L^* -state, 15% are in the M^* -state, and 55% are in the H^* -state. In all cases, the M^* -state is only weakly populated. This implies that the free energy of this state is higher than that of the two others. The population distribution in the presence of AMPPNP is peculiar (28% L^* , 10% M^* , 62% H^*): the FRET levels did not change within the photon bursts, indicating that the enzyme did not carry out catalysis; however, the FRET level maxima corresponded to those of a catalytically active enzyme (see Figures 4 and 6). Therefore, AMPPNP binding traps the enzyme in a ‘frozen catalytic conformation’, which differs from the inactive state.

Discussion

The ϵ -subunit during catalysis

In this work, intramolecular single-molecule FRET was used to investigate the movements of the ϵ -subunit during catalysis in membrane-integrated F_0F_1 . During catalysis, we found characteristic fluctuations of the FRET efficiencies within photon bursts of a single enzyme. The FRET efficiencies remained constant for short time intervals (with dwell times of about 5–150 ms), and then rapidly changed to the next FRET level within 1 ms. A statistical evaluation of the data revealed FRET level histograms with three distinct maxima of the distribution, which were defined the H^* -, the M^* -, and the L^* -level. During ATP hydrolysis and ATP synthesis, these maxima were observed at similar FRET efficiencies; however, the sequence of FRET levels was opposite for both directions of the reaction.

From the mean FRET efficiencies of each level, the distances between the two fluorophores were calculated according to the Förster theory. We combined the three $\epsilon 56$ – $b 64$ distances using the program ‘FRETsg’ (Schröder and Grubmüller, 2003), assuming that the three positions of $\epsilon 56$ were allocated on a circle around the axis of rotation. The positions were spaced by 120° rotational steps, and are indicated by green spheres in Figure 7A. Thereby, the position of the second label on the b -subunits is fixed in three dimensions by the three FRET distances 4.6 nm (H^*), 6.3 nm (M^*), and 7.8 nm (L^*), and is visualized as a red sphere in Figure 7A. We fitted these positions into a homology model of the *E. coli* H^+ -ATP synthase (Engelbrecht and Junge, 1997) with the aligned structure of the $\gamma\epsilon$ -complex (Rodgers and Wilce, 2000). We conclude that the dynamics of FRET level changes indicate a rotational movement of the ϵ -subunit relative to the b -subunit, presumably in 120° steps. In accordance with earlier measurements using the actin filament method (Noji *et al*, 1997), the FRET level sequence ($\rightarrow H \rightarrow M \rightarrow L \rightarrow H$) during ATP hydrolysis corresponds to a counter-clockwise rotation of the ϵ -subunit in the model, when viewed from F_0 (blue arrow in Figure 7A). Consequently, clockwise rotation corresponds to ATP synthesis (yellow arrow in Figure 7A). The fact that not all bursts exhibited the same sequence for ATP hydrolysis (only 81%) and for ATP synthesis (only 84%) is due to the kinetics of catalysis. In our analysis, only levels with more than 4 ms were

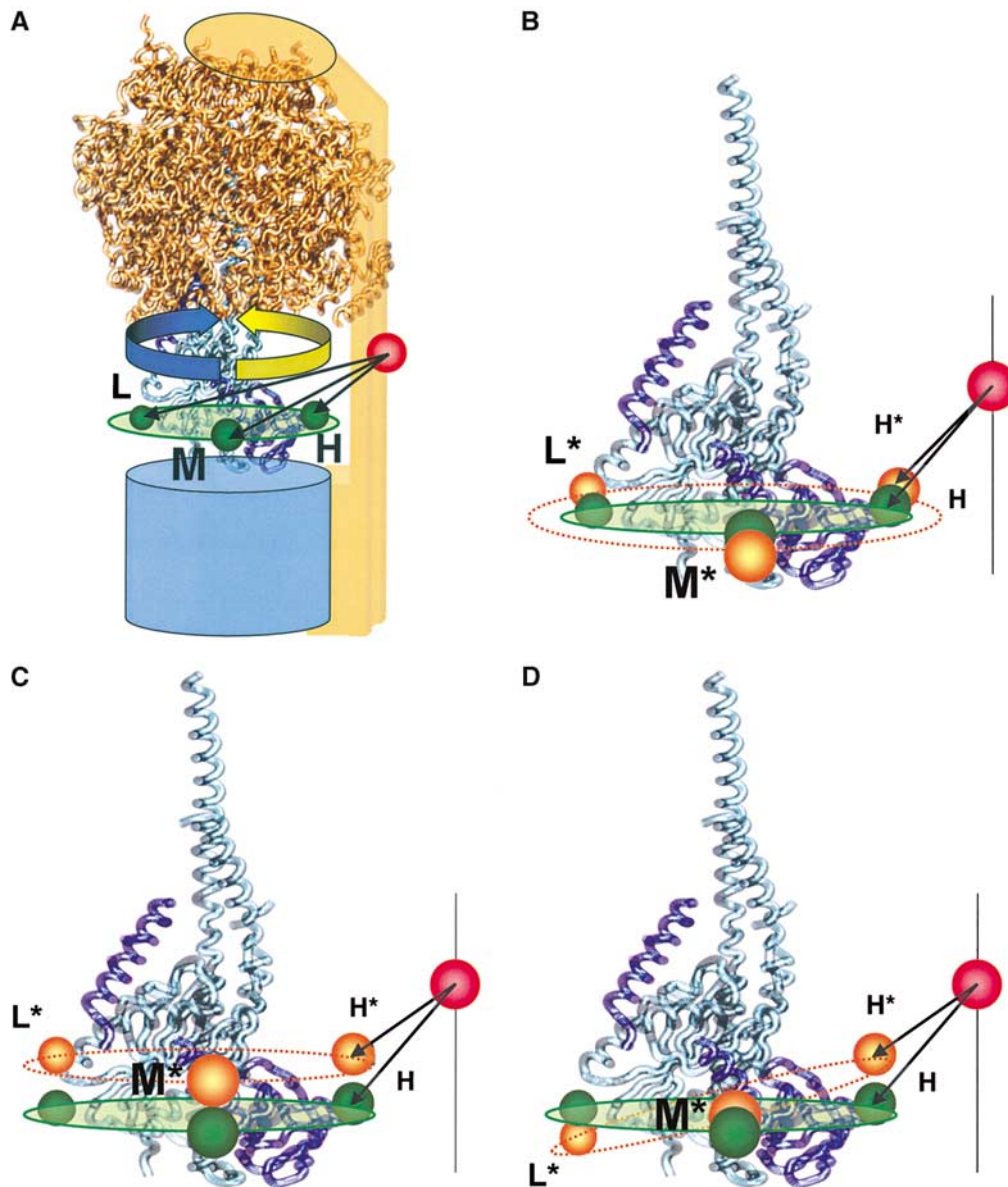


Figure 7 Visualization of the FRET distances in the F_0F_1 model. (A) The three donor–acceptor distances calculated from the FRET efficiencies obtained during catalysis are shown in green and labeled H, M, and L. The ATP synthesis direction is shown by an yellow arrow and ATP hydrolysis direction by a blue arrow. (B–D) The three donor–acceptor distances calculated from the FRET efficiencies of the inactive enzyme are shown in orange and labeled H*, M*, and L*, in addition to the active positions in green. The different active–inactive distance changes in the H-, M-, and L-state by the same conformational change in the $\gamma\epsilon$ -complex. (B) Distance changes by expanding the radius of rotation at $\epsilon 56$. (C) Distance change by shifting perpendicular to the membrane plane. (D) Distance changes by tilting with respect to the membrane plane.

identified as a separate level. Assuming an exponential distribution of the dwell times, we calculated from the average dwell times (see Figure 5) 76% (ATP hydrolysis) and 80% (ATP synthesis) FRET levels with a duration longer than 4 ms. Therefore, apparently wrong sequences could be observed because short levels were not recognized.

Earlier single-molecule investigations of ϵ -movements in immobilized F_1 parts reported a complex behavior. With CF_1 , an irregular stepwise motion of ϵ was observed (Häsler *et al*, 1998). With F_1 from PS3, the rotation of the ϵ -subunit was demonstrated using the fluorescent actin filament as a marker; however, the rate of rotation was a factor 2 lower than that of the γ -subunit under the comparable conditions (Kato-Yamada *et al*, 1998). Presumably, it is complicated to separate

the ϵ -movements resulting from catalysis and those from activation–inactivation of ϵ in immobilized F_1 parts. In single membrane-bound F_0F_1 , a three-stepped rotational movement of ϵ was observed with the same rate as reported earlier for the γ -subunit (Diez *et al*, 2004b), supporting the joint movement of the $\gamma\epsilon$ -complex as expected from ensemble measurements (Aggeler *et al*, 1997).

The same three maxima in the FRET level histograms were found for all catalytic conditions. This indicates that the three resting positions of ϵ relative to the b -subunit are not changed when the enzyme is switched from ATP synthesis to ATP hydrolysis. Two different structures of the isolated ϵ -subunit of F_0F_1 from *E. coli* have been reported (Uhlin *et al*, 1997; Rodgers and Wilce, 2000), and it has been speculated

whether these two conformations might be related to the function of ϵ as a regulatory switch between the directions of catalysis. Several models including up-and-down movements of the C-terminal part of ϵ (Tsunoda *et al*, 2001; Suzuki *et al*, 2003; Bulygin *et al*, 2004), a ratchet-like mechanism with the C-terminus sticking at different angles between α - and β -subunits (Cipriano *et al*, 2002), or an additional ATP binding site (Kato-Yamada and Yoshida, 2003) have been proposed. In our measurements with the catalytically active holoenzyme, the three distances found during ATP synthesis, ATP hydrolysis, and proton transport without nucleotides are very similar. Thus, our data give no evidence for an up-and-down rearrangement of ϵ in the $\epsilon 56$ -region relative to the b -subunit, when the enzyme switches between ATP synthesis and ATP hydrolysis. Of course, we cannot exclude that switching between both modes of catalysis might be connected with movement of other parts of the ϵ -subunit, which does not change the distance between the b -subunit and the $\epsilon 56$ -region.

The movement of the ϵ -subunit during proton translocation in the absence of nucleotides is surprising. We conclude that this might reflect the presence of a 'proton slip' (Feniouk *et al*, 2005). So far, we have detected only a small number of photon bursts with two or more FRET level transitions, which showed significantly increased dwell times of a FRET level as compared to ATP synthesis. However, in contrast to our conclusion, crosslinking data during energization have been interpreted to indicate no rotation of the γ -subunit during energization in the absence of nucleotides (Zhou *et al*, 1997).

AMPPNP inhibits ATP synthesis and hydrolysis, and photon bursts without FRET level changes were observed within the photon bursts (Figure 3A–C). The FRET states exhibited the same FRET efficiencies as during catalysis. We conclude from these data that binding of AMPPNP does not lead to an inactive conformation but it 'freezes' the enzyme in a state with the same ϵ - b distances as during catalysis.

The ϵ -subunit during active–inactive transition

The ϵ -subunit has a dual role in the F_0F_1 -ATP synthase. First, as a part of the rotor, it rotates in 120° steps relative to the b -subunits in the $\alpha_3\beta_3$ -barrel, and second, it regulates the enzyme activity (Sternweis and Smith, 1980; Fischer *et al*, 2000). We analyzed the ϵ - b distances also under conditions where the enzyme did not carry out catalysis. Three FRET states (called H*, M*, and L*) were observed, and the FRET levels did not change during the photon burst, that is, the distances remained constant. However, the mean distances differed from those of the active enzyme. Despite the fact that the corresponding active and inactive FRET levels showed a small overlap of the standard deviations of the Gaussian fits (see Supplementary data), the maxima of the H, M, and L levels for all active conditions, as well as the maxima of the H*, M*, and L* states for the seven inactive conditions, were highly reproducible. Therefore, we conclude that (i) the enzyme has different conformations of ϵ depending on active or inactive conditions and that (ii) the active–inactive transition is connected with a conformational change of ϵ within the central stalk. Three possibilities for the conformational changes associated with the active–inactive transition have to be considered (Figure 7B–D). Assuming that the acceptor position at $b64$ is the same in the active and the inactive state, Figure 7 shows the structural models with the three FRET

distances of the essential γ - ϵ - b section of F_0F_1 . The stopping positions of the $\epsilon 56$ -region as observed in the active state are shown by green spheres, and those observed in the inactive state are shown by orange spheres. The high FRET distance decreased from 4.6 to 4.0 nm, the medium FRET distance remained almost constant (6.3–6.4 nm), and the low FRET distance increased from 7.8 to 8.3 nm. This could be caused by an increase in the radius of rotation for $\epsilon 56$ (Figure 7B). Alternatively, an up-shift of the three ϵ positions during the active–inactive transition including a small inward movement of the $b64$ position (Figure 7C), or a tilting of the plane of rotation for $\epsilon 56$ (Figure 7D), could explain the measured FRET distance changes. Each model could explain the observed changes, or the conformational shift of the $\epsilon 56$ -region has components of all models. It should be mentioned that the conformational changes might lead to differences in mobility or orientation of the transition moments of the fluorophores, which would result also in changes of the energy transfer efficiency. The distances given above do not account for such an effect and should be taken as a first-order approximation. However, the lack of high-resolution structural data for the complete F_0F_1 makes it difficult to describe in detail the conformational changes of ϵ monitoring only one position at $\epsilon 56$ with respect to one position at $b64$.

Functional asymmetry of F_0F_1

According to the binding change theory, each catalytic site adopts sequentially three conformations and works strictly in a cooperative way (Boyer, 1993). This implies that catalysis occurs with the same turnover time at each $\alpha\beta$ -pair. The dwell time represents the docking time of the $\gamma\epsilon$ -complex to one specific $\alpha\beta$ -pair, and we assume that it represents the catalytic turnover time at this $\alpha\beta$ -pair. A detailed analysis of the dwell times of each FRET level separately (see Figure 5, insets) showed that during ATP synthesis as well as during ATP hydrolysis, the dwell time of the M-level is significantly shorter than that of L- and H-level. Correspondingly, the catalytic turnover is higher (between 20 and 30%) than in the two other states. We assume that the relative movement of the subunits is not influenced by the fluorophores since both probes are small. However, we cannot rigorously exclude that there might be an orientation-specific steric hindrance of the rotor movement by the attached TMR.

Three independent results revealed an asymmetry in the function of the enzyme. (i) In the M-level, the catalytic turnover is faster than in the L- and H-level. (ii) Binding of AMPPNP traps the enzyme preferentially in the H-state. (iii) Without catalytic turnover, the enzyme is found preferentially in the L*-state (or H*-state after ATP synthesis or energization) as the inactive states. The reason for this heterogeneity and its significance for the mechanism were not investigated in this work. The interactions of the $\gamma\epsilon$ -complex with the three $\alpha\beta$ -pairs during rotation induce the conformational changes proposed by the binding change theory. One might speculate that the binding of the peripheral stalk $b_2\delta$ to one $\alpha\beta$ -pair leads to some asymmetry in the otherwise identical $\alpha\beta$ -pairs and this gives rise to the observed functional heterogeneities. The b -dimer interacts strongly with one $\alpha\beta$ -pair (Diez *et al*, 2004a; Weber *et al*, 2004), leading to a slightly different conformation of the tagged $\alpha\beta$ -pair (Kersten *et al*, 2000). This $\alpha\beta$ -pair might have smaller activation barriers (M→L for hydrolysis and

M \rightarrow H for synthesis) or a higher Gibbs free energy. It is expected that in the absence of the peripheral stalk, for example, in isolated F_1 parts, this asymmetry is not observed.

In ensemble measurements, neither static nor dynamic heterogeneities within a population of molecules can be detected. In single-molecule enzymology, functional single holoenzymes are investigated selectively, and mechanisms are derived from a statistical analysis. This general approach is applicable to a broad variety of biological systems for monitoring structural dynamics, binding and unbinding, oligomerization, and catalytic processes.

Materials and methods

Purification and labeling of F_1 and F_0F_1 -ATP synthase from *E. coli*

The plasmid pRAP100 carrying the ϵ H56C mutation was constructed from pRA100 (Aggeler and Capaldi, 1992) by Medigenomix (Germany) and expressed in strain RA1. F_1 was isolated as described (Gogol *et al*, 1989). Preparation of F_0F_1 from pRR76, containing the mutation bQ64C expressed in strain RA1, was carried out as described (Börsch *et al*, 2002). The F_0F_1 preparation before labeling contained 1.5 ATP/ F_0F_1 and 0.9 ADP/ F_0F_1 . Protein and fluorophore concentrations were determined by UV absorption. F_1 - ϵ H56C (20 μ M) was labeled with tetramethylrhodamine-C₅-maleimide (TMR; Molecular Probes) with a molar ratio of 1:0.9 in 50 mM MOPS-NaOH (pH 7.0) and 100 μ M MgCl₂ at 0°C for 4 min. The molar ratio of bound fluorophore to protein (54%) was calculated from absorption spectra with correction of the absorption of the fluorophore at 280 nm. The following absorption coefficients were used: $\epsilon_{(555\text{ nm})} = 95\,000\text{ M}^{-1}\text{ cm}^{-1}$, $\epsilon_{(280\text{ nm})} = 19\,000\text{ M}^{-1}\text{ cm}^{-1}$ for TMR (Molecular Probes), and $\epsilon_{(280\text{ nm})} = 191\,000\text{ M}^{-1}\text{ cm}^{-1}$ for F_1 (Gill and von Hippel, 1989). The two b -subunits of F_0 -bQ64C- F_1 (20 μ M) were crosslinked with Cy5bis-C₅-maleimide (Cy5bis; Diez *et al*, 2004b) with a molar ratio of 1:1 in the same buffer as described for F_1 labeling in the presence of 0.1% *n*-dodecylmalto-side (Glycon) at 0°C for 90 min. The labeling efficiency was 94%, as determined from the absorption spectra using $\epsilon_{(650\text{ nm})} = 250\,000\text{ M}^{-1}\text{ cm}^{-1}$ and $\epsilon_{(280\text{ nm})} = 5200\text{ M}^{-1}\text{ cm}^{-1}$ for Cy5bis (Diez *et al*, 2004b), and $\epsilon_{(280\text{ nm})} = 340\,000\text{ M}^{-1}\text{ cm}^{-1}$ for F_0F_1 (Gill and von Hippel, 1989). Selectivity of labeling of F_1 and F_0F_1 was checked by measuring the fluorograms after gel electrophoresis. Approximately 90% of the b -subunits were crosslinked by Cy5bis according to SDS-PAGE. The rate of ATP hydrolysis (v_{H}) of F_1 was measured with an ATP regenerating system (Fischer *et al*, 2000) at 37°C in a buffer containing 100 mM Tris-HCl (pH 8), 25 mM KCl, 4 mM MgCl₂, 2.5 mM phosphoenolpyruvate, 18 U/ml pyruvate kinase, 16 U/ml lactate dehydrogenase, and 0.2 mM NADH.

Preparation of F_0F_1 in a liposome

Labeled (or unlabeled) F_0F_1 was reconstituted into liposomes as described (Fischer and Gräber, 1999). The number of F_0F_1 per liposome was adjusted as follows. The diameter of the liposomes was determined by light scattering yielding 120 ± 10 nm. The sum of inner and outer surfaces of the liposome was 7.9×10^4 nm². Using 0.6 nm^2 (Nagle *et al*, 1996) for the average area of one lipid, the number of lipid molecules was 1.32×10^5 . The lipid concentration during reconstitution was 7.5 g/l or 10 mM. Using 1.32×10^5 lipids per liposome, the liposome (or vesicle) concentration was 75 nM. Addition of 15 nM F_0F_1 resulted in a ratio of five liposomes per F_0F_1 . If the incorporation of F_0F_1 into liposomes occurred statistically, about 80% of the vesicles contained no enzyme, and the number of liposomes containing more than one was negligible. F_0 -liposomes were prepared by stripping the F_1 part (Lötscher *et al*, 1984) as follows: F_0F_1 -liposomes were centrifuged (90 min at 264 000 g, room temperature) and resuspended in 1 mM tricine-NaOH (pH 8.0), 1 mM DTT, 0.5 mM EDTA, and 4% (v/v) glycerol. The resuspended liposomes were incubated for 90 min at room temperature, centrifuged, and resuspended twice. Finally, the stripped vesicles were resuspended in the same buffer to yield an F_0 concentration of 60 nM. The F_0 -liposome suspension (less than one F_0 per liposome) was incubated with labeled (or unlabeled) F_1 at a molar excess of two F_1 per F_0 in the presence of 2.5 mM MgCl₂ and 50 mM NaCl,

first for 45 min at 37°C and then for 90 min at 0°C. The excess of unbound F_1 was removed by three subsequent ultracentrifugation steps (90 min, 264 000 g, 4°C) and by resuspending the pellet in 20 mM tricine-NaOH (pH 8.0), 20 mM succinic acid, 0.6 mM KCl, and 4% (v/v) glycerol. The final concentration of F_0F_1 was adjusted to 40–50 nM.

The rates of ATP hydrolysis (v_{H}) and ATP synthesis (v_{S}) were measured at 23°C to control the efficiency of reconstitution. All activities were calculated on the basis of the F_0 concentration. ATP hydrolysis was carried out with an ATP regeneration system (see above) after preincubation of the F_0F_1 -liposomes with 25 mM KCl for 24 h. ATP synthesis was measured after an acid-base transition in the presence of a K⁺/valinomycin diffusion potential. F_0F_1 -liposomes (30 μ l) were mixed with 120 μ l of a buffer with 20 mM succinic acid-NaOH (pH 4.7), 5 mM NaH₂PO₄, 0.6 mM KOH, 2.5 mM MgCl₂, 100 μ M ADP, and 20 μ M valinomycin. After 3 min incubation, 150 μ l of the acidic suspension was injected into 850 μ l of 200 mM tricine-NaOH (pH 8.8), 5 mM NaH₂PO₄, 160 mM KOH, 2.5 mM MgCl₂, and 100 μ M ADP. The generated ATP was monitored by the luciferin/luciferase assay as described (Turina *et al*, 2003). For specific inhibition of ATP hydrolysis, the proteoliposomes were incubated with 100 μ M DCCD (60 min at 30°C), and with 60 μ M DCCD (60 min at 23°C) for inhibition of ATP synthesis.

Single-molecule fluorescence measurements

Single-molecule fluorescence measurements were performed at room temperature using a home-built two-channel confocal microscope setup (Börsch *et al*, 2002). The intensity of the laser beam (Nd:YAG, 532 nm, Coherent) was attenuated to 105 μ W and fluorescence from FRET-labeled F_0F_1 -liposomes at a final concentration of 50–90 pM was recorded by a multichannel scaler PC-card (PMS 300, Becker&Hickl) using 1 ms binning time. Measurements under various conditions (no substrate, 3 mM phosphate, 1 mM ADP, 1 mM AMPPNP, 1 mM ATP) were carried out in a buffer containing 20 mM tricine-NaOH (pH 8.0), 20 mM succinic acid, 2.5 mM MgCl₂, 0.6 mM KCl, and 4% (v/v) glycerol. Measurements at pH 4.7 were carried out in a buffer containing 20 mM succinic acid-NaOH (pH 4.7), 0.6 mM KOH, 2.5 mM MgCl₂, 3 mM phosphate, and 1 mM ADP. Fluorescence measurements during ATP synthesis were carried out after energization of the F_0F_1 -liposomes (generation of a Δ pH plus $\Delta\phi$ by mixing the same two buffers as described above for bulk measurements of ATP synthesis with two syringes) in a microscopic flow chamber, which was implemented in the confocal setup. Data were recorded for 3 min after mixing. The concentrations of AMPPNP, ADP, and ATP were determined by UV absorption using $\epsilon_{(260\text{ nm})} = 15\,400\text{ M}^{-1}\text{ cm}^{-1}$.

FRET data analysis

The recorded fluorescence intensities were corrected as follows: mean background count rates (usually between 0.5 and 2 kHz), which were obtained from measurements of pure buffer solutions, were subtracted. Additionally, a small leak of donor signal into the acceptor channel ('crosstalk') was measured and taken into account to yield the corrected fluorescence intensities of donor (F_{D}) and acceptor (F_{A}). Mean diffusion times, τ_{D} , through the confocal detection volume of approximately 7 fl were measured by fluorescence correlation spectroscopy (Börsch *et al*, 1998) for the unbound dye ($\tau_{\text{D}} = 0.4$ ms), donor-labeled F_1 (not bound to F_0 , $\tau_{\text{D}} = 3.6$ ms), and labeled F_0F_1 -liposomes ($\tau_{\text{D}} = 25$ ms). Photon bursts with fluorescence intensities above the background were selected by the following criteria: (i) minimal duration longer than 20 ms, and (ii) at least 400 photons as a sum of photon counts in both detection channels.

For each photon burst, the FRET efficiencies were calculated in 1 ms steps when the sum of corrected count rates in both channels was greater than 10 kHz. The FRET efficiency was calculated according to $E_{\text{FRET}} = F_{\text{A}} / (F_{\text{A}} + \gamma F_{\text{D}})$ with a correction factor $\gamma = \eta_{\text{A}}\Phi_{\text{A}} / \eta_{\text{D}}\Phi_{\text{D}}$ where η_{D} and η_{A} are the overall detection efficiencies of the donor and the acceptor channel. Φ_{D} and Φ_{A} are the fluorescence quantum yields of the enzyme-bound donor and acceptor. $\eta_{\text{D}} = 0.35$ and $\eta_{\text{A}} = 0.35$ were calculated by comparing the corrected emission spectra of donor and acceptor with the transmission characteristics of the filters and the spectral sensitivities of the detectors of the single-molecule setup. The quantum yield $\Phi_{\text{D}} = 0.37$ of TMR at ϵ 56 was measured relative to sulforhodamine 101 as a standard (Karstens and Kobs, 1980). For the FRET acceptor Cy5bis, the quantum yield $\Phi_{\text{A}} = 0.32$ was

reported previously (Diez *et al*, 2004b). With these data, we obtain $\gamma = 0.87$.

For photon bursts with changes of the FRET efficiency, a FRET level was recognized when this level remains constant for longer than 4 ms. The mean E_{FRET} values for all levels within all bursts were calculated and were collected in histograms for the different experimental conditions. The peaks in the histograms were approximated by Gaussian distributions, and the maxima were used to calculate the mean distances between the two fluorophores. The relative population of the different FRET states was calculated by integration of the Gaussian fits. When several FRET level were observed within one photon burst (during ATP hydrolysis, during ATP synthesis, and during energization without ADP), the dwell times of the FRET levels were also measured. The first and the last FRET levels were omitted in the dwell time histograms because their duration before entering and after leaving the confocal volume remained unknown. The dwell time histograms were fitted by an exponential function to obtain the average dwell times. Donor-labeled proteoliposomes (about 60% of all bursts) were identified as bursts without photons in the acceptor channel, and were omitted from further data analysis. Liposomes with two labeled F_0F_1 were expected to have a doubled fluorescence intensity. Such bursts (less than 1%) were excluded.

Calculation of intramolecular distances from single-molecule FRET data

Distances (r_{DA}) between the FRET donor and acceptor were calculated according to $r_{\text{DA}} = R_0[(1/E_{\text{FRET}}) - 1]^{1/6}$ (Förster, 1948). FRET efficiencies E_{FRET} were taken from the maxima of Gaussian fits

References

- Aggeler R, Capaldi RA (1992) Cross-linking of the γ subunit of the *Escherichia coli* ATPase (ECF₁) via cysteines introduced by site-directed mutagenesis. *J Biol Chem* **267**: 21355–21359
- Aggeler R, Ogilvie I, Capaldi RA (1997) Rotation of a γ - ϵ subunit domain in the *Escherichia coli* F₁F₀-ATP synthase complex. The γ - ϵ subunits are essentially randomly distributed relative to the $\alpha\beta\beta\delta$ domain in the intact complex. *J Biol Chem* **272**: 19621–19624
- Boldt F-M, Heinze J, Diez M, Petersen J, Börsch M (2004) Real-time pH microscopy down to the molecular level by combined scanning electrochemical microscopy/single molecule fluorescence spectroscopy. *Anal Chem* **76**: 3473–3481
- Börsch M, Diez M, Zimmermann B, Reuter R, Gräber P (2002) Stepwise rotation of the γ -subunit of EF₀F₁-ATP synthase observed by intramolecular single-molecule fluorescence resonance energy transfer. *FEBS Lett* **527**: 147–152
- Börsch M, Turina P, Eggeling C, Fries JR, Seidel CA, Labahn A, Gräber P (1998) Conformational changes of the H⁺-ATPase from *Escherichia coli* upon nucleotide binding detected by single molecule fluorescence. *FEBS Lett* **437**: 251–254
- Böttcher B, Bertsche I, Reuter R, Gräber P (2000) Direct visualisation of conformational changes in EF₀F₁ by electron microscopy. *J Mol Biol* **296**: 449–457
- Böttcher B, Schwarz L, Gräber P (1998) Direct indication for the existence of a double stalk in CF₀F₁. *J Mol Biol* **281**: 757–762
- Boyer PD (1993) The binding change mechanism for ATP synthase—some probabilities and possibilities. *Biochim Biophys Acta* **1140**: 215–250
- Boyer PD (1998) ATP synthase—past and future. *Biochim Biophys Acta* **1365**: 3–9
- Bulygin VV, Duncan TM, Cross RL (1998) Rotation of the ϵ subunit during catalysis by *Escherichia coli* F₀F₁-ATP synthase. *J Biol Chem* **273**: 31765–31769
- Bulygin VV, Duncan TM, Cross RL (2004) Rotor/Stator interactions of the ϵ subunit in *Escherichia coli* ATP synthase and implications for enzyme regulation. *J Biol Chem* **279**: 35616–35621
- Capaldi RA, Aggeler R (2002) Mechanism of the F₁F₀-type ATP synthase, a biological rotary motor. *Trends Biochem Sci* **27**: 154–160
- Cipriano DJ, Bi Y, Dunn SD (2002) Genetic fusions of globular proteins to the ϵ subunit of the *Escherichia coli* ATP synthase: implications for *in vivo* rotational catalysis and epsilon subunit function. *J Biol Chem* **277**: 16782–16790
- Diez M, Börsch M, Zimmermann B, Turina P, Dunn SD, Gräber P (2004a) Binding of the b-subunit in the ATP synthase from *Escherichia coli*. *Biochemistry* **43**: 1054–1064
- Diez M, Zimmermann B, Börsch M, König M, Schweinberger E, Steigmiller S, Reuter R, Felekyan S, Kudryavtsev V, Seidel CA, Gräber P (2004b) Proton-powered subunit rotation in single membrane-bound F₀F₁-ATP synthase. *Nat Struct Mol Biol* **11**: 135–141
- Duncan TM, Bulygin VV, Zhou Y, Hutcheon ML, Cross RL (1995) Rotation of subunits during catalysis by *Escherichia coli* F₁-ATPase. *Proc Natl Acad Sci USA* **92**: 10964–10968
- Engelbrecht S, Junge W (1997) ATP synthase: a tentative structural model. *FEBS Lett* **414**: 485–491
- Feniouk BA, Mulikidjanian AY, Junge W (2005) Proton slip in the ATP synthase of *Rhodobacter capsulatus*: induction proton conduction and nucleotide dependence. *Biochim Biophys Acta* **1706**: 184–194
- Fischer S, Gräber P, Turina P (2000) The activity of the ATP synthase from *Escherichia coli* is regulated by the transmembrane proton motive force. *J Biol Chem* **275**: 30157–30162
- Fischer S, Gräber P (1999) Comparison of ΔpH - and $\Delta\phi$ -driven ATP synthesis catalyzed by the H⁺-ATPases from *Escherichia coli* or chloroplasts reconstituted into liposomes. *FEBS Lett* **457**: 327–332
- Förster T (1948) Zwischenmolekulare Energiewanderung und Fluoreszenz. *Ann Phys* **2**: 55–70
- Gill SC, von Hippel PH (1989) Calculation of protein extinction coefficients from amino acid sequence data. *Anal Biochem* **182**: 319–326
- Gogol EP, Lucken U, Bork T, Capaldi RA (1989) Molecular architecture of *Escherichia coli* F₁ adenosinetriphosphatase. *Biochemistry* **28**: 4709–4716
- Häsler K, Engelbrecht S, Junge W (1998) Three-stepped rotation of subunits γ and ϵ in single molecules of F-ATPase as revealed by polarized, confocal fluorometry. *FEBS Lett* **426**: 301–304
- Junge W (1999) ATP synthase and other motor proteins. *Proc Natl Acad Sci USA* **96**: 4735–4737
- Kaim G, Prummer M, Sick B, Zumofen G, Renn A, Wild UP, Dimroth P (2002) Coupled rotation within single F₀F₁ enzyme complexes during ATP synthesis or hydrolysis. *FEBS Lett* **525**: 156–163

of the FRET level histograms. The Förster radius $R_0 = 64 \text{ \AA}$ for the pair TMR/Cy5 was determined from $R_0 = 0.2111[J(\lambda)n^{-4}\kappa^2\Phi_D]^{1/6}$ as follows: the overlap integral, $J(\lambda)$, was calculated from the emission spectrum of F₁- ϵ H56C-TMR and the absorption spectrum of F₀-bQ64C-Cy5bis-F₁ to yield $J(\lambda) = 9.90 \times 10^{-13} \text{ M}^{-1} \text{ cm}^3$. The donor quantum yield $\Phi_D = 0.37$ was determined as described above. For the index of refraction, $n = 1.33$ was used, and for the orientation factor, $\kappa^2 = 2/3$ was assumed. This value is in the range of possible κ^2 values for the case of linear and planar (due to rotation) transition moments of donor and acceptor (Van der Meer *et al*, 1994). The anisotropies r of the fluorophores bound to the protein were measured for F₁- ϵ H56C-TMR and F₀-bQ64C-Cy5bis-F₁. The data indicate that TMR at $\epsilon 56$ ($r_{\text{TMR}} = 0.06$) can move unrestricted, whereas the mobility of Cy5bis at b64 ($r_{\text{Cy5bis}} = 0.25$) is more restricted.

Supplementary data

Supplementary data are available at *The EMBO Journal* online.

Acknowledgements

We thank CAM Seidel for the gift of the Cy5 dye, W Wangler for excellent technical assistance, A Aird for software solutions, P Turina for inspiring discussions, J Wrachtrup and DJ Cipriano for critical reading of the manuscript, and A Börsch-Haubold for editorial suggestions. The financial support by the Landesstiftung Baden-Württemberg in the network of competence 'functional nanodevices' is gratefully acknowledged.

- Karrasch S, Walker JE (1999) Novel features in the structure of bovine ATP synthase. *J Mol Biol* **290**: 379–384
- Karstens T, Kobs K (1980) Rhodamine B and rhodamine 101 as reference substances for fluorescence quantum yield measurements. *J Phys Chem* **84**: 1871–1872
- Kato-Yamada Y, Noji H, Yasuda R, Kinoshita Jr K, Yoshida M (1998) Direct observation of the rotation of ϵ subunit in F_1 -ATPase. *J Biol Chem* **273**: 19375–19377
- Kato-Yamada Y, Yoshida M (2003) Isolated ϵ subunit of thermophilic F_1 -ATPase binds ATP. *J Biol Chem* **278**: 36013–36016
- Kersten MV, Dunn SD, Wise JG, Vogel PD (2000) Site-directed spin-labeling of the catalytic sites yields insight into structural changes within the F_0F_1 -ATP synthase of *Escherichia coli*. *Biochemistry* **39**: 3856–3860
- Kinoshita Jr K, Adachi K, Itoh H (2004) Rotation of F_1 -ATPase: how an ATP-driven molecular machine may work. *Annu Rev Biophys Biomol Struct* **33**: 245–268
- Lötscher HR, deJong C, Capaldi RA (1984) Modification of the F_0 portion of the H^+ -translocating adenosinetriphosphatase complex of *Escherichia coli* by the water-soluble carbodiimide 1-ethyl-3-[3-(dimethylamino)propyl]carbodiimide and effect on the proton channeling function. *Biochemistry* **23**: 4128–4134
- McLachlin DT, Coveny AM, Clark SM, Dunn SD (2000) Site-directed cross-linking of b to α , β , and a subunits of the *Escherichia coli* ATP synthase. *J Biol Chem* **275**: 17571–17577
- Nagle JF, Zhang R, Tristram-Nagle S, Sun W, Petrache HI, Suter RM (1996) X-ray structure determination of fully hydrated L alpha phase dipalmitoylphosphatidylcholine bilayers. *Biophys J* **70**: 1419–1431
- Noji H, Yasuda R, Yoshida M, Kinoshita Jr K (1997) Direct observation of the rotation of F_1 -ATPase. *Nature* **386**: 299–302
- Rodgers AJ, Wilce MC (2000) Structure of the γ/ϵ complex of ATP synthase. *Nat Struct Biol* **7**: 1051–1054
- Rubinstein JL, Walker JE, Henderson R (2003) Structure of the mitochondrial ATP synthase by electron cryomicroscopy. *EMBO J* **22**: 6182–6192
- Sabbert D, Engelbrecht S, Junge W (1996) Intersubunit rotation in active F-ATPase. *Nature* **381**: 623–625
- Schröder GF, Grubmüller H (2003) FRETsg: biomolecular structure model building from multiple FRET experiments. *Comp Phys Comm* **158**: 150–157
- Smith JB, Sternweis PC (1977) Purification of membrane attachment and inhibitory subunits of the proton translocating adenosine triphosphatase from *Escherichia coli*. *Biochemistry* **16**: 306–311
- Sternweis PC, Smith JB (1980) Characterization of the inhibitory (ϵ) subunit of the proton-translocating adenosine triphosphatase from *Escherichia coli*. *Biochemistry* **19**: 526–531
- Suzuki T, Murakami T, Iino R, Suzuki J, Ono S, Shirakihara Y, Yoshida M (2003) F_0F_1 -ATPase/synthase is geared to the synthesis mode by conformational rearrangement of ϵ subunit in response to proton motive force and ADP/ATP balance. *J Biol Chem* **278**: 46840–46846
- Tang C, Capaldi RA (1996) Characterization of the interface between γ and ϵ subunits of *Escherichia coli* F_1 -ATPase. *J Biol Chem* **271**: 3018–3024
- Tsunoda SP, Rodgers AJ, Aggeler R, Wilce MC, Yoshida M, Capaldi RA (2001) Large conformational changes of the ϵ subunit in the bacterial F_1F_0 ATP synthase provide a ratchet action to regulate this rotary motor enzyme. *Proc Natl Acad Sci USA* **98**: 6560–6564
- Turina P, Samoray D, Gräber P (2003) H^+ /ATP ratio of proton transport-coupled ATP synthesis and hydrolysis catalysed by CF_0F_1 -liposomes. *EMBO J* **22**: 418–426
- Uhlin U, Cox GB, Guss JM (1997) Crystal structure of the ϵ subunit of the proton-translocating ATP synthase from *Escherichia coli*. *Structure* **5**: 1219–1230
- Van der Meer BW, Cooker G, Chen SS-Y (1994) *Resonance Energy Transfer: Theory and Data*. New York: VHC
- Weber J, Senior AE (2003) ATP synthesis driven by proton transport in F_1F_0 -ATP synthase. *FEBS Lett* **545**: 61–70
- Weber J, Wilke-Mounts S, Nadanaciva S, Senior AE (2004) Quantitative determination of direct binding of b subunit to F_1 in *Escherichia coli* F_1F_0 -ATP synthase. *J Biol Chem* **279**: 11253–11258
- Wilkens S, Capaldi RA (1998) ATP synthase's second stalk comes into focus. *Nature* **393**: 29
- Yasuda R, Noji H, Yoshida M, Kinoshita Jr K, Itoh H (2001) Resolution of distinct rotational substeps by submillisecond kinetic analysis of F_1 -ATPase. *Nature* **410**: 898–904
- Yoshida M, Muneyuki E, Hisabori T (2001) ATP synthase—a marvellous rotary engine of the cell. *Nat Rev Mol Cell Biol* **2**: 669–677
- Zhou Y, Duncan TM, Cross RL (1997) Subunit rotation in *Escherichia coli* F_0F_1 -ATP synthase during oxidative phosphorylation. *Proc Natl Acad Sci USA* **94**: 10583–10587